Macromolecules

Article

pubs.acs.org/Macromolecules

Polymer Phase Separation in a Microcapsule Shell

Weichao Shi[†,‡] and David A. Weitz*[,†,‡]

[†]Department of Applied Physics, School of Engineering and Applied Sciences, and [‡]Wyss Institute for Biologically Inspired Engineering, Harvard University, Cambridge, Massachusetts 02138, United States

Supporting Information

ABSTRACT: Phase separation has been used for engineering microscale fluids and particles with designed structures. But it is challenging to use phase separation to create complicated microcapsules because phase separation in the shell correlates with applied osmotic pressure and affects capsule stability significantly. Here we employ two biodegradable polymers to study the phase separation in microcapsule shells and its effect on the mechanical stability. The dynamic process reveals that phase separation creates a patchy shell with distinct regions transiently, then transports the discrete domains across the shell, and coalesces them at the surface. The equilibrium structure with balanced osmotic pressure is a Janus shell, where one component forms the shell and the other component dewets on the surface. Under slight osmotic pressure to the shell, phase separation reaches a different Janus shape, which consists of two partial shells of each component. We can in further take advantage of phase separation and osmotic pressure to rupture microcapsules at specific locations. Phase separation in the shell provides a facile approach to create versatile capsule structures and affords a reliable strategy to harness the shell mechanics.

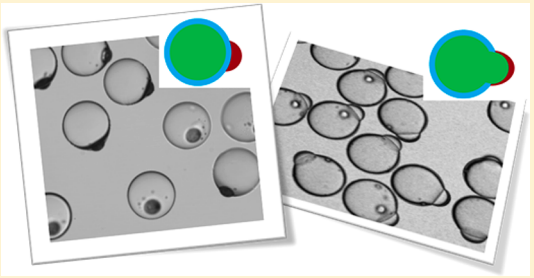

INTRODUCTION

Phase separation creates macroscopic heterogeneity from immiscible components. During a phase separation process, structural evolution is accompanied by mass transport and develops from small length heterogeneities to large separated domains. The thermodynamics and the dynamic evolution of phase separation have been well understood in bulk.[1] Recently, phase separation within microscale fluids has attracted broad attention based on the fast development of microfluidic techniques.[2,3] The liquid drops are typically ∼100 μm in diameter with narrow dispersity. One typical example is the oil-in-water (O/W) single emulsion drops. A large variety of heterogeneous particles (such as Janus spheres, concentric spheres, spheres with multicompartments, and so on) has been achieved by mediating the thermodynamics or the dynamics of phase separation in drops.[4−16] There is another set of special liquid drops, namely double emulsions (for example, water-in-oil-in-water ($W_1/O/W_2$)), from which we get microcapsules by solidifying the oil phase.[17−20] Microcapsules possess efficient ability of encapsulation and release and have been used in foods, pharmaceuticals, cosmetics, and chemical separation.[21−25] Tuning the capsule shell properties with multiple components broadens the range of potential applications. Usually, the shell thickness of microcapsules is quite small (∼1 μm) compared with the coarsened domains after phase separation. In this case, phase separation takes place more likely in a 2D soft shell, which is significantly different from the phase separation in bulk or in single emulsion drops. In addition, phase separation in the shell is closely correlated with the shell stability, mainly based on two factors: one is the osmotic pressure applied to the shell (osmotic difference between W_1 and W_2);[20,26,27] the other is the mass transport in the shell during phase separation.[1,28] The mechanical instability has been a bottleneck to process microcapsules with complex shell structures. A fundamental understanding of phase separation in the microcapsule shell is thus the key to explore new capsule structures and high throughput synthesis of stable microcapsules for various application purposes.

Here we study the phase separation of two biodegradable polymers in a microcapsule shell. Under balanced osmotic pressure, the thermodynamics of a partially wetting interface always prefers a Janus shell structure, where a shell of component A is attached by a small domain of component B. In comparison, phase separation under slight osmotic pressure creates a different type of Janus structure spontaneously, where a partial shell of component A connects to another partial shell of component B. The mechanical instability of the shell accompanied by phase separation is well overcome in our study. In addition, we can take advantage of the heterogeneous structures and osmotic pressure to rupture microcapsules at specific locations. The fundamental understanding and methods used in this study provide general guidelines to synthesize microcapsules with complex structures through phase separation and to make use of the phase separation to control the mechanical behavior of microcapsules.

Received: June 14, 2017
Revised: September 8, 2017

DOI: 10.1021/acs.macromol.7b01272
Macromolecules XXXX, XXX, XXX−XXX

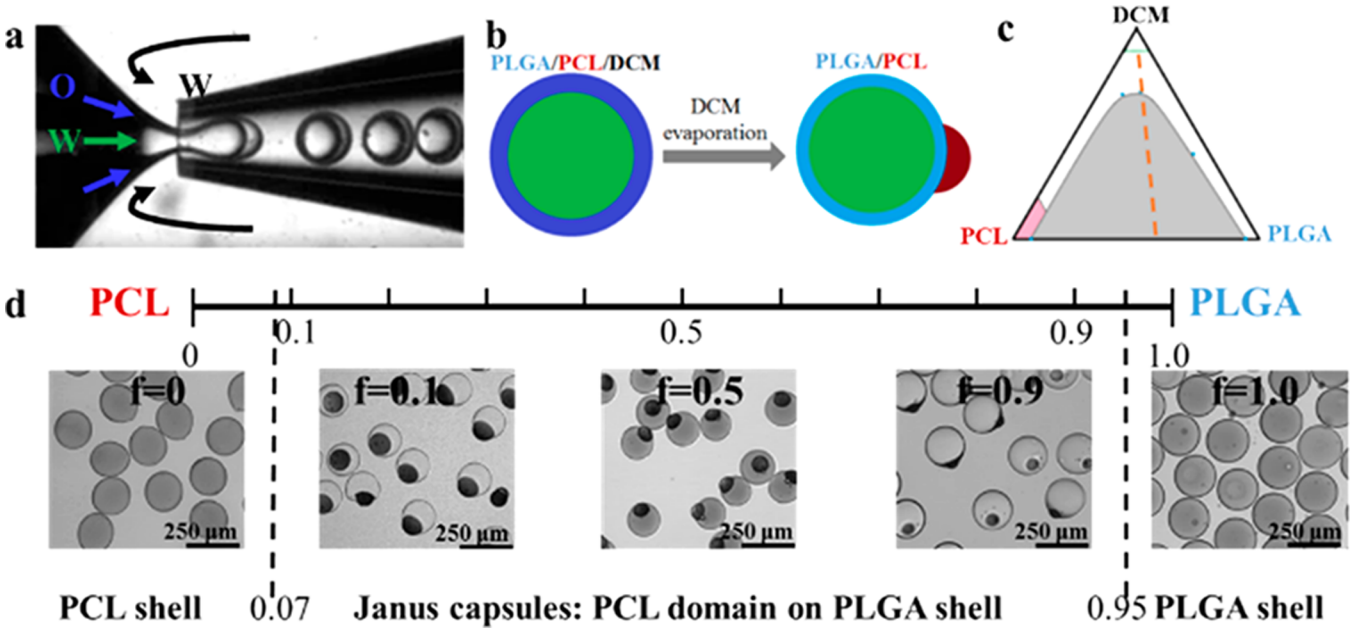

Figure 1. Phase separation in the microcapsule shell under balanced osmotic pressure. (a) Geometry of glass capillaries for microcapsule processing. (b) Schematic illustration of a W/O/W microcapsule and the formation of a Janus structure. The oil phase constitutes PLGA, PCL, and DCM and is homogeneous in the initial state (dark blue). By evaporation of DCM, PLGA and PCL start phase separation and finally reach to a Janus structure with a PCL domain (red) on PLGA shell (light blue). (c) A measured phase diagram of PLGA/PCL/DCM ternary system. (d) Experimental results of microcapsule structures at different PLGA concentrations. The infusion rates of the inner/middle/outer fluids are 1/1/5 mL/h for all experiments. DCM is evaporated slowly from a sealed vial with small holes in the lid.

EXPERIMENTAL SECTION

Two circular glass capillaries and a rectangular glass capillary are used for making devices. Two circular capillaries have outer diameters of 1.00 mm and are thermally pulled to break on a Flaming/Brown Micropipet Puller machine (Model P-97, Sutter Instrument Co.), which produces a sharp tip for each glass capillary. The tips are further polished to certain sizes with a sand paper. For injection tube, the outer diameter of the tip is about 60 μm; for collection tube, the outer diameter is 120 μm. The inner surface of the injection tube is treated by a silane (1 wt % of (heptadecafluoro-1,1,2,2-tetrahydrodecyl)-trimethoxysilane in Novec 7500) for 30 min. The collection tube is used directly without chemical modification. The rectangular capillary has an inner diameter of 1.05 mm. Two circular glass capillaries are inserted into the rectangular glass capillary and aligned to the same axis. The gap between the inject and collection capillaries is about 60 μm. Two needles are fixed by epoxy resin for the injection of the middle and outer fluids from two ends of the rectangular capillary. The inner and middle fluids are pinched off by the outer fluid between two capillaries to produce W/O/W double emulsion drops.

The inner and outer fluids are both 6 wt % poly(vinyl alcohol) (PVA, 13−23 kg/mol, 87−89% hydrolyzed, Sigma-Aldrich) aqueous solution. To assist fluorescent imaging, 0.01 mg/mL fluorescein isothiocyanate−dextran (500 kg/mol, Sigma-Aldrich) is added into the inner fluid. The excitation wavelength is 488 nm. The emission is collected from 490 to 540 nm.

The middle fluid has two polymers, polycaprolactone (PCL, 45 kg/mol, Sigma-Aldrich) and poly(lactic-*co*-glycolic acid) (PLGA, 30−50 kg/mol, Sigma-Aldrich). The two polymers are dissolved in dichloromethane (DCM), which is a good solvent for both. The weight fraction of DCM is 90 wt % for all experiments, while the weight ratio of the two polymers varies. A fluorescent reagent, Nile red (Sigma-Aldrich), is added with 0.01 mg/mL to assist imaging. The excitation wavelength is 543 nm. The emission is collected from 570 to 660 nm.

During drop processing, the infusion flow rate is controlled by syringe pumps (Harvard Apparatus). The real-time drop production is observed using an inverted microscope (Leica) equipped with a high-speed camera (Phantom V9.0). The phase separation dynamics and Janus microcapsule formation are observed with a confocal optical microscope (Leica TCS SP5).

RESULTS AND DISCUSSION

Phase Separation with Balanced Osmotic Pressure. The water-in-oil-in-water ($W_1/O/W_2$) double emulsions are processed using microfluidic techniques in glass capillary devices (Supporting Information Figure S1). The device geometry is shown in Figure 1a. The inner and outer fluids are both 6 wt % poly(vinyl alcohol) (PVA) aqueous solution. The middle fluid has two biodegradable polymers, polycaprolactone (PCL) and poly(lactic-*co*-glycolic acid) (PLGA), dissolved in dichloromethane (DCM), which is a good solvent for both. The weight fraction of DCM is 90 wt % for all experiments, while the weight ratio of the two polymers varies. The size and shell thickness of microcapsules are mediated by the infusion rates of the inner, middle, and outer fluids. The fabricated microcapsules are collected in 6 wt % PVA solution.

The capsules are solidified through a solvent evaporation process. The solvent dissolves into water and then evaporates. As it does so, the total polymer concentration increases in the shell. Above a certain concentration, liquid−liquid phase separation takes place between the two dissolved polymers, and a Janus structure is formed, where a PCL-rich domain is attached to the PLGA-rich shell. The phase transformation is schematically illustrated in Figure 1b. The Janus structure is solidified by further evaporation of DCM, forming a PLGA hard shell with a crystallized PCL domain.

We depict the phase diagram for PCL/PLGA/DCM, determined experimentally, in Figure 1c. The initial state of the oil phase is at 90 wt % DCM, indicated by the green line. Through solvent evaporation, the system evolves along the dashed orange line and enters the phase separation region (the gray area), where two liquid phases coexist. Since PCL is a

DOI: 10.1021/acs.macromol.7b01272
Macromolecules XXXX, XXX, XXX−XXX

crystalline polymer, the PCL-rich phase transforms to a crystal structure when the concentration of PCL is over ~80 wt % in that phase. The crystallization region of PCL is indicated by light red. However, because the liquid−liquid phase separation with Janus capsule formation is completed much earlier before crystallization fixes the structure, we ignore the crystallization process for the purposes of this study.

Three typical structures are created through this process. When the polymer weight fraction of PLGA is less than 0.07, PCL forms the shell; when it is higher than 0.95, PLGA forms the shell; in the intermediate composition range, Janus microcapsules are harvested, where PLGA forms the shell and a PCL domain is attached at the surface. The structures of the microcapsules are presented in Figure 1d for different PLGA concentrations.

The formation of Janus microcapsules in such a broad composition range is counterintuitive to the traditional understanding of polymer phase separation in bulk systems, where sea−island or bicontinuous structures usually form.[1] We would expect to see similar structures in microcapsules. Especially when PLGA is the minority component, we would expect the nucleation of PLGA discrete domains and the appearance of a reversed Janus structure, where a PLGA domain attaches on the PCL shell. However, the nucleation of PLGA discrete domains occurs only in a very narrow concentration range from 0.05 to 0.07 (Figure S2). Given that we are observing phase separation in a shell of less than 10 μm thickness and in a water medium, the unique capsule structures indicate that interfacial properties dominate phase separation.

Phase separation tends to locally minimize the interfacial energy of a microcapsule. For the purposes of this discussion, the structure of a microcapsule can be determined by interfacial tensions between liquid phase A to water (γ_{AW}), liquid phase B to water (γ_{BW}), and phase A to phase B (γ_{AB}). This analysis is usually described using spreading coefficients,[3] defined as

$$S_i = \gamma_{jk} - (\gamma_{ij} + \gamma_{ik}) \quad (1)$$

There are three spreading coefficients, S_A, S_B, and S_W, corresponding to each microcapsule structure. Suppose γ_{AW} is smaller than γ_{BW}, so $S_B < 0$. Given that, we should expect three possible structures: (a) for $S_A > 0$ and $S_W < 0$, phase B is completely engulfed in a shell of A; (b) for $S_A < 0$ and $S_W < 0$, phase B partially wets the A shell; and (c) for $S_A < 0$ and $S_W > 0$, phase B completely dewets from the A shell. The resulted capsule structures are illustrated in Figure 2a−c, respectively. The Janus microcapsule formation in this study is described by the second case, where A corresponds to the PLGA-rich liquid phase and B to the PCL-rich liquid phase. We verify this claim by measuring the interfacial tensions γ_{AW} and γ_{BW} relative to γ_{AB} in our experiment. Based on Neumann's triangle analysis (Figure 2d),[3] $\gamma_{AW} = \gamma_{AB} \sin(180° - 126°)/\sin(180° - 138°) = 1.21\gamma_{AB}$ and $\gamma_{BW} = \gamma_{AB} \sin(180° - 96°)/\sin(180° - 138°) = 1.49\gamma_{AB}$. Since $\gamma_{AW} < \gamma_{BW}$, forming a shell of phase A lowers the free energy of a Janus microcapsule.

Phase Separation Pathway and Microcapsule Stability. From the perspective of thermodynamics, the total interfacial energy of a microcapsule is not at the global minimum, which leads to significant stability concerns under perturbation. For the phase separation in the shell, perturbation arises from the mass transport of coarsening domains. We observe the phase separation dynamics under microscope

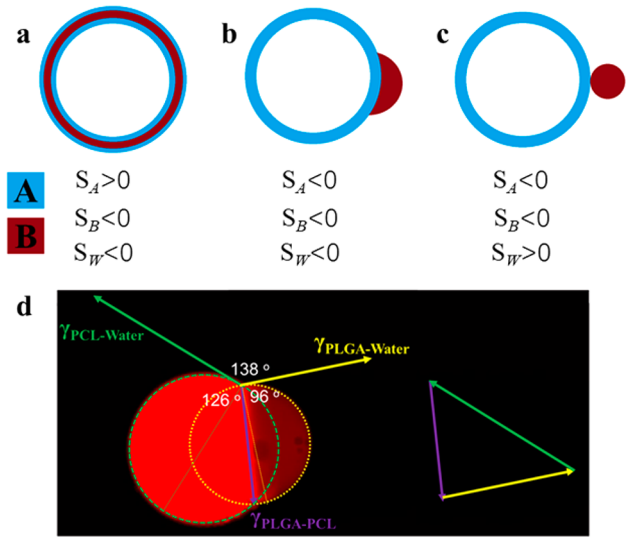

Figure 2. Equilibrium microcapsule structures predicted by spreading coefficients. Blue and red indicate phase A and B, respectively, and $\gamma_{AW} < \gamma_{BW}$. (a) An A/B/A sandwich shell, (b) phase B partially wetting the A shell, and (c) phase B completely dewetted from the A shell. (d) Contact angle analysis of interfacial tensions of PCL−water (green), PLGA−water (yellow), and PLGA−PCL (purple), which is measured in a Janus single emulsion drop. The solvent, polymer concentration, and the PVA solution are controlled in the same condition with double emulsions for Neumann's triangle analysis.

(Supporting Information Movie S1). The solvent DCM evaporates from the shell and triggers phase separation. Small domains emerge, transport, and coalesce quickly at the shell surface. The microcapsules are mostly intact when the shell thickness is large and significant rupture takes place later in the solvent evaporation process when the shell is thin (Figure S3). We further observe the capsule stability at different shell thickness, where capsules are processed at a given concentration. We vary the infusion ratios of the inner and middle fluids to tune the shell thickness in the liquid state (Figure S4). We find that when shells are thin, almost no microcapsules remain intact after solvent evaporation; when shells are thick, capsule yield increases. So, there is a relationship between shell thickness, phase separation, and capsule stability.

To look into the dynamic evolution, we capture the intermediate structures by fast solvent evaporation from the shell. During such a process, the polymers solidify quickly and dynamically trap the phase separating structures in the shell. The surface morphology in Figure 3a indicates that capsules possess heterogeneous structures, where discrete domains randomly distribute in the shell. This type of structure is also known as patchy microcapsules.[29−31] We can also remove the "patches" and produce porous shells (Figure 3b). As shown previously by Kim et al.,[17] phase separation in the shell provides an easy approach to create porous capsules.

On the basis of the experimental results, we infer that phase separation creates heterogeneous domains in the shell transiently, and those domains transport across the shell and coalesce on the surface to generate a Janus shape. During phase separation, small domains in the shell move to the shell surface, coalesce to decrease interfacial energy, and create the Janus shape, as predicted by the spreading coefficients in Figure 2b. To reach such a thermodynamic state, there are several possible dynamic pathways. Rupture of the microcapsules is more likely to correlate with the pathway that how a domain leaves the

DOI: 10.1021/acs.macromol.7b01272
Macromolecules XXXX, XXX, XXX−XXX

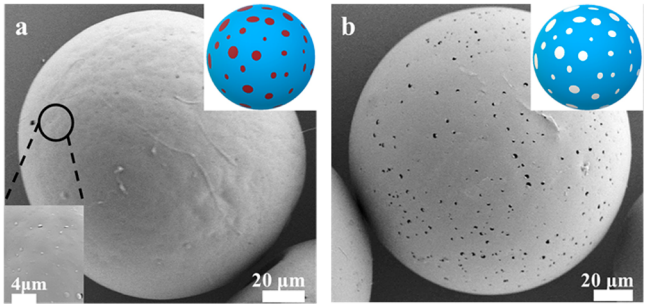

Figure 3. Intermediate state of phase separation in the microcapsule shell. (a) Structure of a patchy microcapsule, which is a transient state during phase separation. (b) Structure of a porous microcapsule, which is obtained by removing the discrete domains from the patchy shell.

shell to the surface. To supplement the experimental findings and generalize the understanding of capsule stability, we calculate the free energy change in the possible dynamic coarsening processes. For a small domain with radius R and height h, it would leave the shell either by a hopping with a defect left on the shell (from state 1 to state 2 as shown in Figure 4a) or by a smooth migration (from state 1 to state 3). It

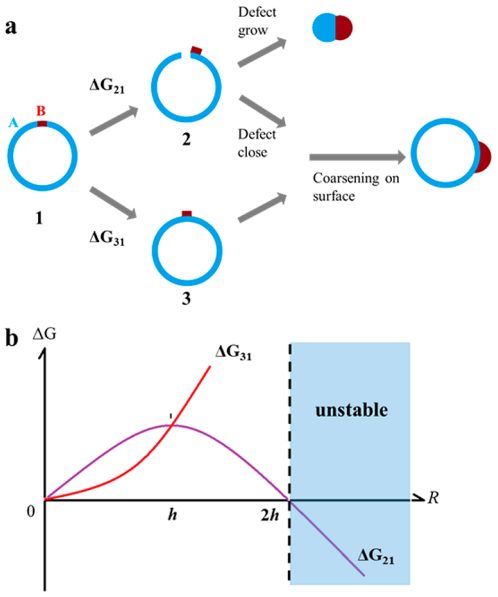

Figure 4. Effect of domain transport on capsule stability. (a) Two possible dynamic pathways of domain transportation across the shell. (b) The corresponding energy curves of ΔG_{21} and ΔG_{31}.

should be noted that the pathway through either state 2 or state 3 targets to the same Janus microcapsule structure (Figure 2b). But the dynamic pathway through state 3 always produces stable capsules, while the transient state 2 might result in rupture when defects are created spontaneously. The energy changes in the two cases are written respectively as

$$\Delta G_{21} = \pi S_W R^2 - 2\pi h S_W R \quad (2)$$

$$\Delta G_{31} = -\pi S_A R^2 + 2\pi h(\gamma_{BW} - \gamma_{AB})R \quad (3)$$

The brief derivation is given in the Supporting Information (part E). Keeping in mind that the spreading coefficients must be $S_A < 0$, $S_B < 0$, and $S_W < 0$ in a Janus microcapsule formation, then ΔG_{21} is negative when $R > 2h$, and state 2 is thermodynamically preferred over state 1. The energy curve is illustrated in Figure 4b. The energy barrier to initiate a defect is $-\pi S_W h^2$, which increases with the square of the shell thickness. So, microcapsules with thin shells tend to get over the energy barrier and rupture under small perturbations (Figure S6). ΔG_{31} is always positive when $R > 0$, and transition through state 3 is not spontaneous. Notably, when the domain size is very small, the transition to state 3 is possible with a slight energy penalty, but the energy cost increases quickly with the radius of the domain.

The coarsening of phase separation is expected to happen such that when the domain size is small, it prefers coarsening in the shell, but it is still possible that very small domains could transport to the surface. In this case, the microcapsule is mechanically stable during phase separation. So, we could dynamically trap this state (state 1 as shown in Figure 3a) by quickly evaporating the solvent from the shell. When the domain size is large enough, transport to the outer surface by leaving a defect in the shell is preferred, which leads to rupture of microcapsule. This explanation qualitatively agrees with our experimental results.

As discussed above, there is energy barrier to transport discrete domains across the shell. Here we consider the possible driving force to generate the transport. Regarding the dynamics of phase separation, for a small domain with dimension ~1 μm and an interfacial tension of ~10^{-2} N/m, the energy barrier $-\pi S_W h^2$ of domain transport across the shell is on the order of 10^{-14} J, which is much larger than thermal energy (~10^{-21} J) or gravitational energy (~10^{-20} J). So, thermal and gravitational effects are both negligible for the domain transport across the shell. The most probable driving force comes from interfacial tension itself, which drives hydrodynamic flow due to local curvature variation (Siggia's mechanism).[28]

The discussion above suggests that to harvest stable microcapsules through phase separation, the key is to reduce the possibility of creating defects in the shell. One straightforward idea is to fabricate microcapsules with thick shells so that the critical defect size in state 2 is too large to achieve during phase separation. Instead, domain transport over the shell may proceed to state 3. Another important factor is to have solvent evaporate slowly, which prevents large perturbations with hydrodynamic effects. By controlling these conditions, Janus microcapsules can be harvested with less than 10% lost due to rupture.

Phase Separation with Applied Osmotic Pressure. We further study the phase separation in a microcapsule shell under osmotic pressure. For the $W_1/O/W_2$ double emulsions, the osmotic pressure can be mediated in two aqueous solutions independently. At balanced osmotic pressure, phase separation always creates a Janus shape (type I), where PLGA form the shell and a PCL domain attaches on the surface. There is a contact area between the two phases, where stress is not uniformly distributed. The balance can be maintained throughout phase separation until the whole structure solidifies. However, when the osmotic pressure difference increases, such a Janus shape of type I is not the equilibrium structure anymore. Instead, a new type of Janus microcapsule (type II) is generated (Figure 5).

Tracking the dynamic evolution under a slight osmotic difference (~5000 Pa between 6% PVA as the inner solution and 8% PVA as the outer), we find that phase separation first creates the Janus capsules of type I, where a PCL domain dewets on the PLGA shell. Since PLGA-rich phase forms the

DOI: 10.1021/acs.macromol.7b01272
Macromolecules XXXX, XXX, XXX−XXX

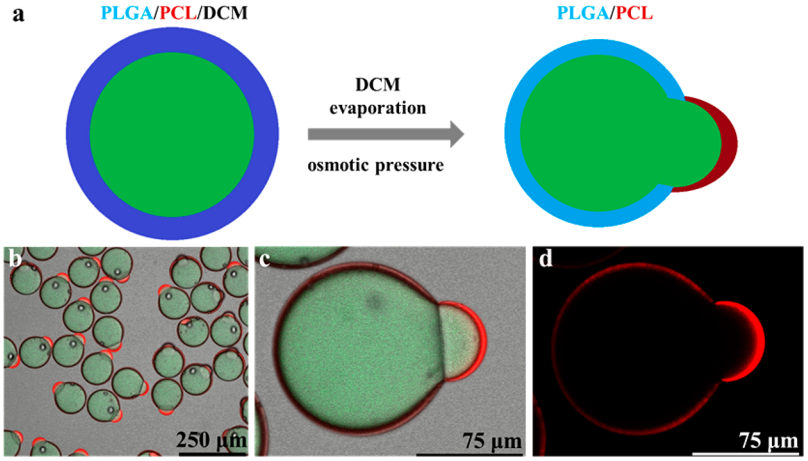

Figure 5. Phase separation in the microcapsule shell under slight osmotic pressure. (a) Schematic illustration of the microcapsule structure from the initial homogeneous state to phase-separated state under applied osmotic pressure. Images b–d are taken using confocal optical microscope. Fluorescence of the shell is from Nile red, and that of the inner aqueous phase is from FITC (green color). Nile red is initially homogeneous in PCL/PLGA/DCM in the shell. After phase separation, Nile red remains preferentially in the PCL-rich phase, which is more hydrophobic than the PLGA-rich phase. (b, c) Overlaid images from Nile red, FITC, and optical channels. (d) The Nile red channel for the shell envelope.

shell, there is large interfacial area to evaporate the solvent DCM and thus solidifies quickly. In contrast, the dewetted PCL-rich domain has less interfacial area to evaporate the solvent and thus solidifies slowly. Under imbalanced osmotic pressure, there is applied stress to the shell. The weakest part of the shell, which is at the contact region, is slowly broken, and the stress balance needs to be rebuilt. Then, we observe that the inner water phase tends to decrease in volume, and meanwhile, the PCL domain pushes outward slowly and forms a partial shell to the larger PLGA shell, like a swelling "balloon" filled by water. Finally, the microcapsule reaches the equilibrium state where the Janus capsule (type II) consists of two partial shells of PLGA and PCL, respectively (more evidence is given in Figure S7 and Movie S2).

As explained before, the Janus structure of type I is thermodynamically preferred to minimize local free energy. From a thermodynamics perspective, we do not expect to create the Janus microcapsule of type II, where the total interfacial energy increases by increasing the contact area between PCL and water and meanwhile decreasing the contact area between PLGA and PCL. The energy gain is paid by osmotic pressure. Observing the evolution of the capsule radii (Figure S8), we find that the radius of the PCL partial shell decreases, which indicates the Laplace pressure increases by $\Delta P = 2\gamma_{PCL-water}(1/R_2 - 1/R_1)$, where and R_1 and R_2 are radius of the PCL partial shell before and after shape transformation. Given $\gamma_{PCL-water} = 10^{-2}$ N/m, $\Delta P = 2900$ Pa, which is on the same scale as the osmotic pressure applied.

It should be noted that the phase-separated Janus shells are not stable any more under even larger osmotic pressure. The failure of the microcapsules always starts at the contact area, either by rupturing the interface between PCL and PLGA (Figure S9 and Movie S3) or by buckling the area to form a concave region (Figure S10 and Movie S4). The former happens when the inner aqueous solution has a larger osmotic pressure, and the latter case occurs in the opposite condition. So, phase separation under large osmotic pressure provides an easy approach to harness the mechanical stability of the microcapsules, which is useful for the application of controlled cargo release.

CONCLUSIONS

In summary, we study phase separation of PCL and PLGA in microcapsule shells using microfluidic techniques. Phase separation first creates patchy microcapsules with distinct regions in the shell, and then discrete domains transport across the shell and coalesce at the surface. The equilibrium structure is a Janus shell (type I) to minimize the total interfacial energy, where a PCL domain dewets on a PLGA shell. The domain transport across the shell results in significant challenge to achieve stable microcapsules. The stability problem can be overcome by controlling shell thickness and solvent evaporation. Under slight osmotic pressure, phase separation experiences a similar dynamic pathway but finally reaches a different Janus structure (type II), where a PCL partial shell connects to a PLGA partial shell. Under larger osmotic pressure, Janus microcapsules have mechanical failure always at the contact area in the shell. Harnessing phase separation in the shell provides a facile one-step approach to create versatile capsule structures. Although this study is carried out specifically in PCL/PLGA polymer systems, the fundamental understanding and methods used in this study provide general guidelines to exploit phase separation for microcapsule synthesis and mechanics control, which is the basis for high throughput engineering of microcapsules in industry.

ASSOCIATED CONTENT

Supporting Information

The Supporting Information is available free of charge on the ACS Publications website at DOI: 10.1021/acs.macromol.7b01272.

Part A: geometry of the glass capillary device; part B: nucleation of PLGA discrete domains in PCL shell; part C: capsule thickness variation during solvent evaporation; part D: capsule stability at different infusion ratios of inner and middle fluids; part E: brief derivation of the energy curves; part F: energy curves of unstable coarsening at different shell thickness; part G: structure of type II Janus microcapsules under SEM; part H: evolution of capsule radii during formation of the second type of Janus microcapsules; part I: rupture of Janus

DOI: 10.1021/acs.macromol.7b01272
Macromolecules XXXX, XXX, XXX−XXX

microcapsules at the contact areas; part J: buckling of Janus microcapsules at the contact areas (PDF)
Movie S1: Phase separation in microcapsule shells and the mechanical instability (AVI)
Movie S2: Phase separation under applied osmotic pressure (AVI)
Movie S3: Capsule rupture at the contact area (AVI)
Movie S4: Capsule buckling at the contact area (AVI)

AUTHOR INFORMATION

Corresponding Author

*E-mail weitz@seas.harvard.edu (D.A.W.).

ORCID

Weichao Shi: 0000-0003-4625-4797
David A. Weitz: 0000-0001-6678-5208

Notes

The authors declare no competing financial interest.

ACKNOWLEDGMENTS

W.S. thanks Dr. Jonathan Didier at the Wyss Institute for Biologically Inspired Engineering for critical reading of the manuscript. This work was supported by the National Science Foundation (DMR-1310266), the Harvard Materials Research Science and Engineering Center (DMR-1420570), the Wyss Institute for Biologically Inspired Engineering at Harvard University, and the BASF Aktiengesellschaft Alliance Agreement.

REFERENCES

(1) Bates, F. Polymer-polymer phase behavior. *Science* **1991**, *251*, 898−905.
(2) Shah, R. K.; Shum, H. C.; Rowat, A. C.; Lee, D.; Agresti, J. J.; Utada, A. S.; Chu, L. Y.; Kim, J. W.; Fernandez-Nieves, A.; Martinez, C. J.; Weitz, D. A. Designer emulsions using microfluidics. *Mater. Today* **2008**, *11*, 18−27.
(3) Pannacci, N.; Bruus, H.; Bartolo, D.; Etchart, I.; Lockhart, T.; Hennequin, Y.; Willaime, H.; Tabeling, P. Equilibrium and non-equilibrium states in microfluidic double emulsions. *Phys. Rev. Lett.* **2008**, *101*, 164502.
(4) Zarzar, L. D.; Sresht, V.; Sletten, E. M.; Kalow, J. A.; Blankschtein, D.; Swager, T. M. Dynamically reconfigurable complex emulsions via tunable interfacial tensions. *Nature* **2015**, *518*, 520−524.
(5) Rozynek, Z.; Mikkelsen, A.; Dommersnes, P.; Fossum, J. O. Electroformation of Janus and patchy capsules. *Nat. Commun.* **2014**, *5*, 3945.
(6) Choi, C. H.; Weitz, D. A.; Lee, C. S. One step formation of controllable complex emulsions: from functional particles to simultaneous encapsulation of hydrophilic and hydrophobic agents into desired position. *Adv. Mater.* **2013**, *25*, 2536−2541.
(7) Liang, F.; Zhang, C.; Yang, Z. Rational design and synthesis of Janus composites. *Adv. Mater.* **2014**, *26*, 6944−6949.
(8) Zhao, Y.; Gu, H.; Xie, Z.; Shum, H. C.; Wang, B.; Gu, Z. Bioinspired multifunctional Janus particles for droplet manipulation. *J. Am. Chem. Soc.* **2013**, *135*, 54−57.
(9) Haase, M. F.; Brujic, J. Tailoring of high-order multiple emulsions by the liquid-liquid phase separation of ternary mixtures. *Angew. Chem., Int. Ed.* **2014**, *53*, 11793−11797.
(10) Min, N. G.; Ku, M.; Yang, J.; Kim, S. H. Microfluidic production of uniform microcarriers with multicompartments through phase separation in emulsion drops. *Chem. Mater.* **2016**, *28*, 1430−1438.
(11) Urban, M.; Freisinger, B.; Ghazy, O.; Staff, R.; Landfester, K.; Crespy, D.; Musyanovych, A. Polymer Janus nanoparticles with two spatially segregated functionalizations. *Macromolecules* **2014**, *47*, 7194−7199.
(12) Sun, Y.; Liang, F.; Qu, X.; Wang, Q.; Yang, Z. Robust reactive Janus composite particles of snowman shape. *Macromolecules* **2015**, *48*, 2715−2722.
(13) Liu, B.; Liu, J.; Liang, F.; Wang, Q.; Zhang, C.; Qu, X.; Li, J.; Qiu, D.; Yang, Z. Robust anisotropic composite particles with tunable Janus balance. *Macromolecules* **2012**, *45*, 5176−5184.
(14) Wang, Y.; Zhang, C.; Tang, C.; Li, J.; Shen, K.; Liu, J.; Qu, X.; Li, J.; Wang, Q.; Yang, Z. Emulsion interfacial synthesis of asymmetric Janus particles. *Macromolecules* **2011**, *44*, 3787−3794.
(15) Li, Z.; Lee, D.; Rubner, M. F.; Cohen, R. E. Layer-by-layer assembled Janus microcapsules. *Macromolecules* **2005**, *38*, 7876−7879.
(16) Deng, R.; Liu, S.; Liang, F.; Wang, K.; Zhu, J.; Yang, Z. Polymeric Janus particles with hierarchical structures. *Macromolecules* **2014**, *47*, 3701−3707.
(17) Kim, B.; Lee, T. Y.; Abbaspourrad, A.; Kim, S. H. Perforated microcapsules with selective permeability created by confined phase separation of polymer blends. *Chem. Mater.* **2014**, *26*, 7166−7171.
(18) Kim, S. H.; Shum, H. C.; Kim, J. W.; Cho, J. C.; Weitz, D. A. Multiple polymersomes for programmed release of multiple components. *J. Am. Chem. Soc.* **2011**, *133*, 15165−15171.
(19) Wu, Y.; Lin, X.; Wu, Z.; Möhwald, H.; He, Q. Self-propelled polymer multilayer Janus capsules for effective drug delivery and light-triggered release. *ACS Appl. Mater. Interfaces* **2014**, *6*, 10476−10481.
(20) Datta, S. S.; Abbaspourrad, A.; Amstad, E.; Fan, J.; Kim, S. H.; Romanowsky, M.; Shum, H. C.; Sun, B.; Utada, A. S.; Windbergs, M.; Zhou, S. 25th anniversary article: double emulsion templated solid microcapsules: mechanics and controlled release. *Adv. Mater.* **2014**, *26*, 2205−2218.
(21) Shimanovich, U.; Bernardes, G. J.; Knowles, T. P. J.; Cavaco-Paulo, A. Protein micro-and nano-capsules for biomedical applications. *Chem. Soc. Rev.* **2014**, *43*, 1361−1371.
(22) Zhang, Y.; Chan, H. F.; Leong, K. W. Advanced materials and processing for drug delivery: the past and the future. *Adv. Drug Delivery Rev.* **2013**, *65*, 104−120.
(23) Ammala, A. Biodegradable polymers as encapsulation materials for cosmetics and personal care markets. *Int. J. Cosmet. Sci.* **2013**, *35*, 113−124.
(24) Vericella, J. J.; Baker, S. E.; Stolaroff, J. K.; Duoss, E. B.; Hardin, J. O., IV; Lewicki, J.; Glogowski, E.; Floyd, W. C.; Valdez, C. A.; Smith, W. L.; Satcher, J. H., Jr.; et al. Encapsulated liquid sorbents for carbon dioxide capture. *Nat. Commun.* **2015**, *6*, 6124.
(25) Shum, H. C.; Kim, J. W.; Weitz, D. A. Microfluidic fabrication of monodisperse biocompatible and biodegradable polymersomes with controlled permeability. *J. Am. Chem. Soc.* **2008**, *130*, 9543−9549.
(26) Kim, S. H.; Park, J. G.; Choi, T. M.; Manoharan, V. N.; Weitz, D. A. Osmotic-pressure-controlled concentration of colloidal particles in thin-shelled capsules. *Nat. Commun.* **2014**, *5*, 3068.
(27) Datta, S. S.; Kim, S. H.; Paulose, J.; Abbaspourrad, A.; Nelson, D. R.; Weitz, D. A. Delayed buckling and guided folding of inhomogeneous capsules. *Phys. Rev. Lett.* **2012**, *109*, 134302.
(28) Siggia, E. D. Late stages of spinodal decomposition in binary mixtures. *Phys. Rev. A: At., Mol., Opt. Phys.* **1979**, *20*, 595−605.
(29) Evers, C. H.; Luiken, J. A.; Bolhuis, P. G.; Kegel, W. K. Self-assembly of microcapsules via colloidal bond hybridization and anisotropy. *Nature* **2016**, *534*, 364−368.
(30) Bollhorst, T.; Rezwan, K.; Maas, M. Colloidal capsules: nano- and microcapsules with colloidal particle shells. *Chem. Soc. Rev.* **2017**, *46*, 2091−2126.
(31) Loiseau, E.; Niedermair, F.; Albrecht, G.; Frey, M.; Hauser, A.; Rühs, P. A.; Studart, A. R. Strong microcapsules with permeable porous shells made through phase separation in double emulsions. *Langmuir* **2017**, *33*, 2402−2410.

DOI: 10.1021/acs.macromol.7b01272
Macromolecules XXXX, XXX, XXX−XXX